Journal of Advanced Research 21 (2020) 25–34

Contents lists available at ScienceDirect

Journal of Advanced Research

journal homepage: www.elsevier.com/locate/jare

# Investigation of adsorption, dissociation, and diffusion properties of hydrogen on the V (1 0 0) surface and in the bulk: A first-principles calculation

Jiayao Qin [a,1], Chongyan Hao [a,1], Dianhui Wang [a,b], Feng Wang [a,b], Xiaofeng Yan [a], Yan Zhong [a,b], Zhongmin Wang [a,b,*], Chaohao Hu [a,b,*], Xiaotian Wang [c,*]

[a] School of Materials Science and Engineering, Guilin University of Electronic Technology, Guilin 541004, PR China
[b] Guangxi Key Laboratory of Information Materials, Guilin University of Electronic Technology, Guilin 541004, PR China
[c] School of Physical Science and Technology, Southwest University, Chongqing 400715, PR China

## HIGHLIGHTS

- Interaction between H and V surface and bulk are fully studied.
- H coverage (θ) effects the adsorption energy of H/V(1 0 0).
- H solubility and diffusivity depend slightly on the H concentration.

## GRAPHICAL ABSTRACT

Schematic of H permeation of dense metallic membrane.

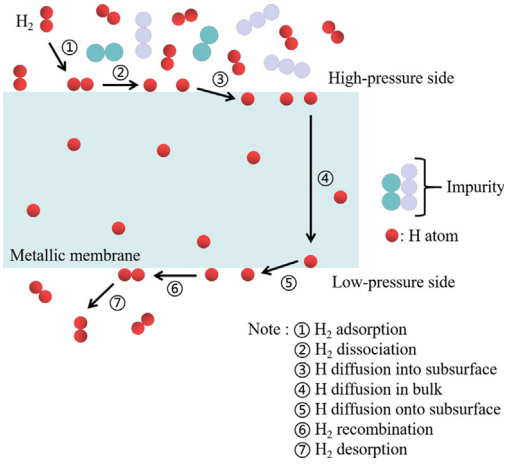


## ARTICLE INFO

*Article history:*
Received 5 August 2019
Revised 13 September 2019
Accepted 16 September 2019
Available online 21 September 2019

*Keywords:*
Hydrogen separation
Vanadium membrane

## ABSTRACT

To investigate the $H_2$ purification mechanism of V membranes, we studied the adsorption, dissociation, and diffusion properties of H in V, an attractive candidate for $H_2$ separation materials. Our results revealed that the most stable site on the V (1 0 0) surface is the hollow site (HS) for both adsorbed H atoms and molecules. As the coverage range increases, the adsorption energy of $H_2$ molecules first decreases and then increases, while that of H atoms remains unchanged. The preferred diffusion path of atoms on the surface, surface to first subsurface, and first subsurface to second subsurface is HS → bridge site (BS) → HS, BS → BS, and BS → tetrahedral interstitial site (TIS) → BS, respectively. In the V bulk, H atoms occupy the energetically favourable TIS, and diffuse along the TIS → TIS path, which has

Peer review under responsibility of Cairo University.

* Corresponding authors at: School of Materials Science and Engineering, Guilin University of Electronic Technology, Guilin 541004, PR China (Z. Wang and C. Hu); School of Physical Science and Technology, Southwest University, Chongqing 400715, PR China (X. Wang).
*E-mail addresses:* zmwang@guet.edu.cn (Z. Wang), chaohao.hu@guet.edu.cn (C. Hu), xiaotianwang@swu.edu.cn (X. Wang).
[1] These authors contributed equally to this work.

https://doi.org/10.1016/j.jare.2019.09.003
2090-1232/

Diffusion kinetics
Adsorption

a lower energy barrier. This study facilitates the understanding of the interaction between H and metals and the design of novel V-based alloy membranes.



## Introduction

Energy resource exhaustion is among the most important challenges facing humankind, and the development of new energy sources has become urgent worldwide. $H_2$, a safe, green, and environmentally friendly renewable energy source, is considered one of the best alternatives to fossil fuels in the future [1,2]. The production, purification, and storage of $H_2$ have always attracted considerable research attention. Separation and purification techniques of $H_2$ determine the application standards of $H_2$ fuel [2–4]. To meet the industrial demand for high-purity $H_2$, $H_2$ purification is necessary. Currently, industrial methods for $H_2$ recovery mainly include membrane separation, pressure-swing adsorption, and cryogenic separation [4,5]. Membrane separation is considered the most promising third-generation gas separation technology, after pressure-swing adsorption and cryogenic separation, because it is economical, convenient, efficient, and clean. Moreover, $H_2$-selective metallic membranes have received much attention for purification. Although Pd-based metallic membranes are the most mature and widely used materials in current research, they are disadvantageous for large-scale production because they are high in cost [6]. Consequently, many researchers have searched for alternatives to reduce costs. Group VB metals (V, Nb, and Ta) have received significant attention because they show better hydrogen permeability, higher mechanical strengths, and lower costs than Pd-based metals [7,8].

V, which has the highest H diffusion coefficient among group VB metals, is currently considered promising as a $H_2$ separation material [5,9]. In addition, V and its alloys are not only considered important $H_2$ storage materials with a large H capacity [8], but also candidate materials for the first walls and blankets of fusion reactors because of their excellent low activation characteristics under neutron irradiation, remarkable high-temperature performance, and swelling resistance under neutron radiation [10]. Until now, many researchers have performed many experiments and theoretical studies on V-based permeable membrane materials, mainly concentrating on the bulk [10–16]. For instance, a work by Dolan et al. showed that a Pd catalyst layer-coated 0.25 mm V substrate membrane exhibited a high permeability under $H_2$ permeation testing, especially at $\geq$320 °C, initially exceeding $3.0 \times 10^{-7}$ mol $m^{-1}$ $s^{-1}$ $Pa^{-1/2}$; the thick-walled membrane was self-supporting and pinhole-free [11]. Luo et al. [13] theorised that H atoms would preferentially occupy tetrahedral interstitial sites (TISs) for greater stability than that offered by octahedral interstitial sites (OISs) or substitutional sites; the corresponding formation energies of occupation were −0.374, −0.226, and +1.83 eV. A theory by Zhang et al. [10] and first-principles exploration by Gui et al. [14] of the trapping mechanism of H vacancies in solid V both showed that single H atoms preferentially occupy sites near the OIS instead of vacancy centre sites; in addition, mono-vacancy sites can trap as many as 12 H or six $H_2$ species. Several fundamental aspects of the interaction between atoms or molecules and solid surfaces are not yet fully understood, such as the mechanism of surface-coverage adsorption.

To our knowledge, preparing clean V surfaces for experiments is difficult and time-consuming [6,17,18]. Studies in the literature that theoretically calculate the H behaviour on V surfaces are limited, despite the interactions between atoms or molecules and solid surfaces being of interest to several industries, especially in heterogeneous catalysis, gas corrosion, separation, and crystal growth [19–22]. Therefore, to provide further insight into the mechanism of H and metal interaction, the mechanisms of H permeation processes have been investigated in detail for metallic membranes.

In this study, we systematically studied the adsorption and diffusion properties of H atoms on the V surface by using first-principles methods. Specifically, all possible stable positions, diffusion energy barriers, and electronic properties of H atoms adsorbed on the V (1 0 0) surface were calculated [23–27], as well as the solution energy and diffusion energy barrier of H in bulk V. We also considered the calculation of adsorption structures from low coverage to high coverage. This work is of great significance for a comprehensive understanding of the mechanism by which H atoms interact with metal surfaces; it provides a theoretical basis for further research on V-based alloys for $H_2$ storage and $H_2$ separation and purification applications.

## Materials and methods

All calculations were performed using the Vienna Ab initio Simulation Package code [28,29]. Perdew–Burke–Ernzerhof generalised gradient approximation functions [30] and the projected augmented wave method [31,32] were used to treat the core–electron interactions. V is a VB group transition metal element, and its valence electron structure with H is $3d^3 4s^2$ and $1\ s^1$, respectively. The kinetic cut-off energy of 360 eV was applied to all systems. The Brillouin zone was sampled by a grid of *k*-points with the resolution $2\pi \times 0.03$ Å$^{-1}$. During geometric optimisation, the energy difference tolerance was less than $1 \times 10^{-6}$ eV atom$^{-1}$ and the force interacting on each atom was less than $1 \times 10^{-2}$ eV Å$^{-1}$. To search the minimum diffusion paths and transition states of the H atom, we employed the climbing image nudged-elastic-band (CI-NEB) method to calculate the H diffusion energy barriers between the optimised initial and final sites [33].

To optimise the computational cost and the accuracy of the DFT calculations, we built a seven-layer slab of the $(2 \times 2)$ V (1 0 0) surface with a vacuum region of 15 Å. Atoms in the upper three V layers were allowed to relax, while those in the bottom four layers were fixed at their bulk positions. The H atoms were placed at the top site (TS), bridge site (BS), and hollow site (HS) in the V surface. The TIS, OIS, and diagonal interstitial site (DIS) were considered for the diffusion of H atoms in the subsurface and bulk, for which $2 \times 2 \times 2$, $3 \times 3 \times 3$, and $4 \times 4 \times 4$ supercell models containing 16, 54, and 128 V atoms, respectively, were built.

The change in the interlayer distance between the slab and bulk model is given by [27]

$$\Delta d = \frac{d_{i-j} - d_0}{d_0} \quad (1)$$

where $d_0$ and $d_{i-j}$ are the interlayer distances between the *i*th and *j*th layers of the slab model before and after relaxation, respectively. Positive $\Delta d$ indicates expansion between the layers, while negative $\Delta d$ indicates contraction.

The surface energy $\gamma_s$ is an important parameter for describing the basic properties of a metal surface, including the surface stability as well as physical and chemical reactions. A lower surface energy indicates better structural stability. It is defined as [34]

$$\gamma_S = \frac{1}{2A}(E_S^{unrelax} - NE_b) + \frac{1}{A}(E_S^{relax} + E_S^{unrelax}) \quad (2)$$

where $E_S^{unrelax}$, $E_S^{relax}$, $E_b$, $A$, and $N$ represent the total energy of the pre-relaxation model, total energy of the model after relaxation, bulk energy per atom, surface area of the cut surface structure, and number of atoms in the slab, respectively.

The average adsorption energy ($E_{ads}$) of H atoms is expressed as [6,27]

$$E_{ads}^{H_2} = \frac{1}{N}(E_{slab+N(H_2)} - E_{slab} - NE_{H_2}) \quad (3)$$

$$E_{ads}^{H} = \frac{1}{N}(E_{slab+N(H)} - E_{slab} - NE_{H}) \quad (4)$$

Here, $E_{slab+H_2}$ and $E_{slab+H}$ are the total energies of the $H_2$-adsorbed system, $E_{slab}$ is the total energy of the slab, $N$ is the number of $H_2$ molecules or H atoms adsorbed, and $E_{H_2}$ and $E_H$ are the total energies of free $H_2$ molecules and H atoms, respectively. Lower H molecular or atomic adsorption energies correspond to more stable adsorption positions.

The solution energy ($E_{sol}$) of the interstitial H atom in bulk bcc V can be obtained as [9,10,13,14]

$$E_{sol}^{H} = E_{NV+H} - E_{NV} - \frac{1}{2}E_{H_2} \quad (5)$$

where $E_{NV+H}$ and $E_{NV}$ are the total energies of the supercell with one H atom and no H atom, respectively. $N$ represents the number of V atoms and $E_{H_2}$ is the total energy of one $H_2$ molecule.

The H diffusion coefficient is given by using the Arrhenius diffusion equation [9,19,22]:

$$D = D_0\, exp\left(-\frac{E_a}{kT}\right) \quad (6)$$

where $D_0$, $E_a$, $T$, and $k$ are the pre-exponential factor, diffusion energy barrier (activation energy), absolute temperature, and Boltzmann constant, respectively.

The equilibrium H concentration is calculated according to Sieverts's law [9,19]:

$$C_H = \left(\frac{P}{P_0}\right)^{\frac{1}{2}} exp\left(-\frac{E_S}{kT} + \frac{\Delta S}{k}\right) \quad (7)$$

where $P$, $P_0$, $E_S$, $\Delta S$, $T$, and $k$ denote the background pressure, reference pressure, solution energy, solution entropy, absolute temperature, and Boltzmann constant, respectively.

To determine the structural properties of bcc V, the equilibrium lattice constant was 2.996 Å for bcc V, which agrees with other theoretical (2.998 Å) [35] and experimental (3.03 Å) [36] values. Moreover, the calculated elastic constants ($C_{11}$ = 262.9, $C_{12}$ = 136.7, and $C_{44}$ = 38.7 GPa) and elastic moduli ($B$ = 178.8, $E$ = 130.0, and $G$ = 47.1 GPa) also agree with both experimental and theoretical results.

## Results and discussions

### Surface model

To obtain a reliable and stable surface, we selected the V (1 0 0) surface of four to nine atomic layers for geometric relaxation. The calculated changes in the interlayer relaxation and surface energies are listed in Table 1. It is seen that the change in the relaxation of the distance between the first and second atomic layer ($\delta d_{1-2}$) values is greater, while the other layer distance changes are slightly weaker. The $\delta d_{1-2}$ values are negative, indicating that the surface atomic layers are contracted, while the $\delta d_{3-4}$ values excluding the five-slab model are positive, showing that the surface atomic layers are expanded. In addition to the surface energy of the seven-slab model agreeing with the experimental result, we observe that the surface energy of the other slab model tends to stabilise at 0.150 eV/Å$^2$ as the thickness of the slab increases in general; this is consistent with the calculated values [37]. Therefore, the seven-slab model can be utilised for further study. Because the H permeation process is not affected by periodicity, the interaction between adjacent surfaces must be eliminated; this is usually achieved by adding a vacuum layer. We tested a series of different thicknesses and found that a 15 Å vacuum layer along the surface normal direction (Z-axis) meets our requirements. To summarise, a slab model of seven atomic layers with a 15 Å vacuum layer is used for further research of the V (1 0 0) surface.

### Adsorption energy

To determine the stability of H atom adsorption sites in the V (1 0 0) surface, we investigated the possible adsorption sites of a single H atom, as shown in Fig. 1(a–k). For the bcc metal (1 0 0) surface, H is mainly adsorbed at surface sites including the TS, BS, and HS. Additionally, H is mainly adsorbed at the first and second subsurface sites, such as the TIS, OIS, and DIS. The calculated absorption energies of the H atoms at these sites are presented in Table 2. It can be seen that the HS has a stronger absorption energy of −2.945 eV among all TSs, BSs, and HSs under a molecular layer (ML) surface coverage of 0.25; their vertical distances from the surface are 1.725, 1.228, and 0.564 Å, respectively, which implies that H prefers to adsorb at the HS. For the subsurface adsorption sites, we can see in Table 2 that TIS (1) has a minimum adsorption energy of −2.407 eV; those of TIS (2) and DIS (1) are respectively −2.275 eV and −2.214 eV; and that of OIS (1) is −2.065 eV; therefore, H is preferentially adsorbed at TIS (1). Similarly, TIS (3) shows a minimum adsorption energy in the second subsurface, which indicates that H-binding sites are energetically stable. In the analysis above, H atoms are most strongly attached to the surface compared to the first and second subsurfaces. In addition, our calculated values show consistency with those reported in the literature [38].

**Table 1**
Calculated interlayer relaxation and surface energies of V (1 0 0) surface as a function of slab thickness.

| Slab model | V (1 0 0) | | | | |
|---|---|---|---|---|---|
| | $\delta d_{1-2}$ (%) | $\delta d_{2-3}$ (%) | $\delta d_{3-4}$ (%) | $\gamma_S$ (eV/Å$^2$) | $\gamma_S$ (J/m$^2$) |
| 5 layers | −15.83 | 2.08 | −0.48 | 0.150 | 2.39 |
| 6 layers | −14.46 | −0.34 | 2.57 | 0.150 | 2.39 |
| 7 layers | −13.82 | −0.02 | 2.72 | 0.152 | 2.44 |
| 8 layers | −15.39 | 0.19 | 2.29 | 0.150 | 2.39 |
| 9 layers | −15.56 | −0.10 | 2.31 | 0.150 | 2.39 |
| Cal. [37] | −12.41 | 0.24 | 2.87 | | 2.40 |
| Exp. [37] | −6.67 | 0.99 | | | 2.55 |

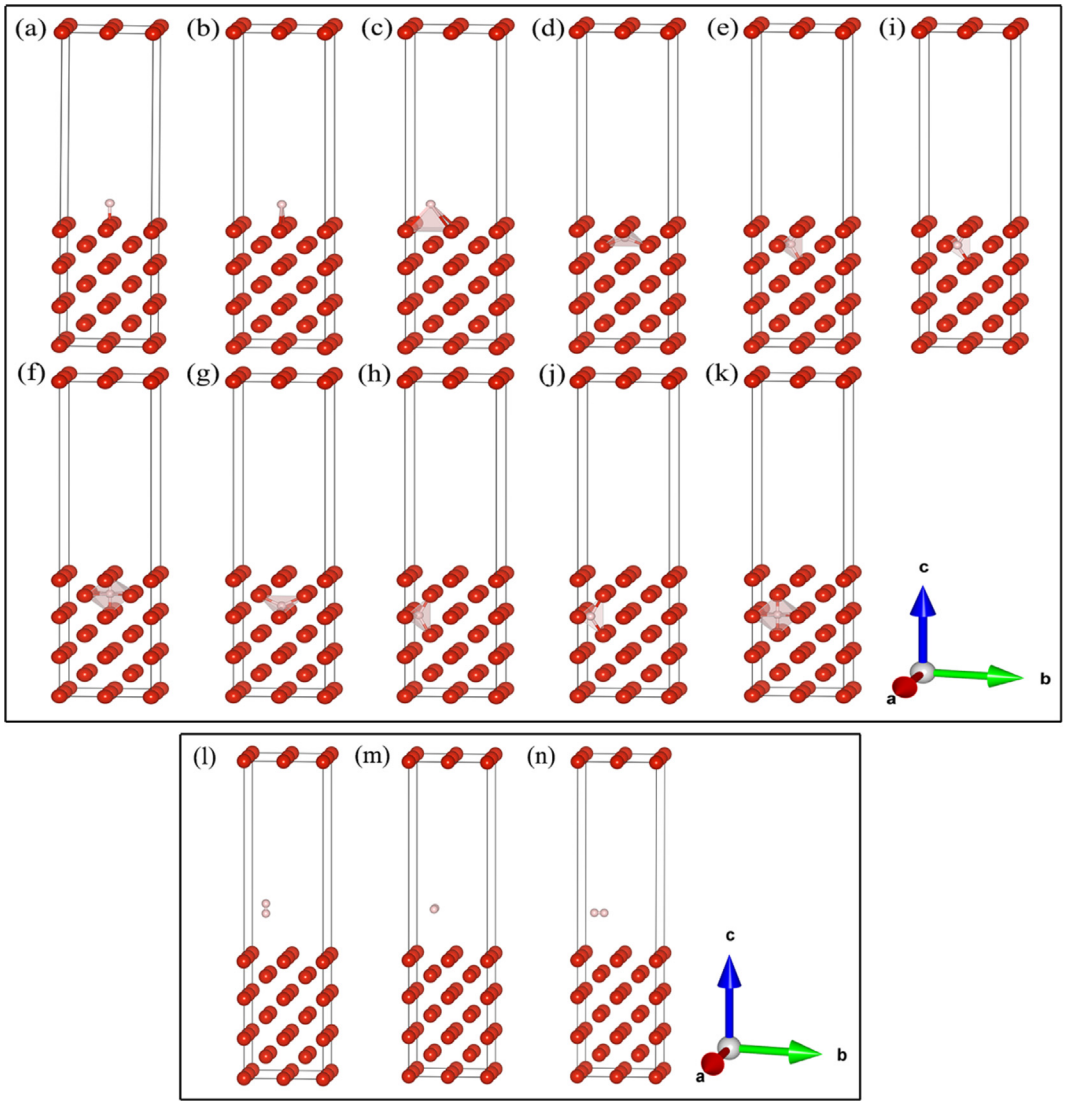


**Fig. 1.** Schematic of H atom and $H_2$ molecular adsorption models with the following possible adsorption sites on the V (1 0 0) surface. Surface: (a) Top site (TS), (b) bridge site (BS), (c) hollow site (HS); first subsurface: (d) tetrahedral interstitial site (TIS) (1), (e) TIS (2), (f) diagonal interstitial site (DIS) (1), (g) octahedral interstitial site (OIS) (1); second subsurface: (h) TIS (3), (i) TIS (4), (j) DIS (2), (k) OIS (2). For $H_2$ molecular adsorption on the V (1 0 0) surface: (l) perpendicular surface orientation (*a* state), (m) parallel lattice constant *a*-axis orientation (*b* state), (n) parallel lattice constant *b*-axis orientation (*c* state).

We further studied the interaction between $H_2$ and the V (1 0 0) surface, where the initial configuration of $H_2$ was first divided into vertical versus parallel to the V (1 0 0) surface. Fig. 1(l–n) shows the adsorption model of the HS, which is labelled as *a*, *b*, and *c* states in our study. Based on the previous calculation results, the vertical distance of a single H atom adsorbed on the surface of V (1 0 0) is about 0.564–1.725 Å, so the distance between the centre of the $H_2$ molecule at the initial position and the surface ($d_{H_2\text{-surf}}$) is set as 1.725 Å. The calculation results we obtained are presented in Table 3. The H—H bond length ($d_{H-H}$) is ~0.751–0.753 Å, almost equal to our calculation for that of free $H_2$ (0.75 Å), indicating that $H_2$ is not dissociated and is adsorbed to the surface in molecular form. This is because the V atoms on the surface are very far away from $H_2$ at this initial distance with only a weak interaction that does not break the H–H bond. The vertical height between the $H_2$ molecule and V surface is ~3.468–4.370 Å. Compared to the *b* and *c* states, molecular $H_2$ is preferentially adsorbed at the TS, BS, and HS in the *a* state with corresponding adsorption energies of −0.001, −0.003, and −0.005 eV, respectively. This demonstrates that the interaction between $H_2$ and the V surface is exothermic and that the adsorption energy of the HS is much smaller than those of the other sites, further indicating that $H_2$ is more inclined to adsorb on the HS of the (1 0 0) surface. However, the TS shows the same adsorption energy of −0.001 eV for a molecule oriented in a parallel or perpendicular manner.

*Electronic properties*

To investigate the electronic properties of H atom absorption at the TS, BS, and HS, we calculated the total density of states (TDOS) and the project density of states, as well as the charge density difference, as depicted in Fig. 2. Fig. 2(a) shows that the peak position of the TDOS and the splitting of the peak are significantly different after the adsorption of H atoms, and that the TDOS of H adsorption at different sites clearly varies. Significant hybridisation occurs between the H *s* and V *d* states, and the V *s*/*p*/*d* states overlap with the H *s* state below the Fermi level. In comparison to the TS and BS, the TS has a clear peak at −6 to −7.5 eV, indicating a strong chemical interaction between H and V atoms. Furthermore, we calculated the Z-direction planar-averaged charge density differences,

**Table 2**
Calculation results for H adsorbed on V (1 0 0) surfaces at 0.25 ML: adsorption energy ($E_{ads}$), short distance between H atom and V atom ($d_{H-V}$), and adsorbate height ($d_{H-surf}$).

| | Site | $E_{ads}$ (eV) | $d_{H-V}$ (Å) | $d_{H-surf}$ (Å) |
|---|---|---|---|---|
| Surface | TS | −2.160 | 1.725 | 1.725 |
| | BS | −2.826 | 1.834 | 1.228 |
| | HS | −2.945 (−2.97) [38] | 1.846 | 0.564 |
| First subsurface | TIS (1) | −2.407 (−2.43) [38] | 1.761 | |
| | TIS (2) | −2.275 | 1.706 | |
| | OIS (1) | −2.065 | 1.634 | |
| | DIS (1) | −2.214 | 1.671 | |
| Second subsurface | TIS (3) | −2.309 (−2.29) [38] | 1.723 | |
| | TIS (4) | −2.477 | 1.728 | |
| | OIS (2) | −2.275 | 1.658 | |
| | DIS (2) | −2.347 | 1.674 | |

**Table 3**
Calculation results of $H_2$ adsorbed on V (1 0 0) surfaces at 0.25 ML.

| Direction | Site | $E_{ads}$ (eV) | $d_{H-H}$ (Å) | $d_{H_2-surf}$ (Å) |
|---|---|---|---|---|
| *a* state | TS | −0.001 | 0.753 | 3.478 |
| | BS | −0.003 | 0.753 | 3.473 |
| | HS | −0.005 | 0.753 | 3.476 |
| *b* state | TS | −0.001 | 0.753 | 3.475 |
| | BS | 0.006 | 0.752 | 3.475 |
| | HS | 0.004 | 0.751 | 4.370 |
| *c* state | TS | −0.001 | 0.753 | 3.468 |
| | BS | 0.006 | 0.753 | 3.475 |
| | HS | 0.008 | 0.751 | 3.908 |

as indicated in Fig. 2(b). The cyan and yellow regions mark areas of charge depletion and accumulation, respectively [39]. Charge redistribution largely occurs between the nearest-neighbour layer V atoms and the H atom interfacial region; at the bottom layer of the V atom, farther from the H atom, almost no charge change is observed. A positive value indicates electron accumulation, while a negative value indicates electron depletion [40]. Accordingly, the electrons are transferred from the V (1 0 0) surface side to the H-atom side. To quantify the change in charge density, we also employed Bader charge analysis, which showed that the H atoms at the TS, BS, and HS have 0.4757, 0.5507, and 0.5965 e, respectively. As far as we know, more negatively charged H atoms have lower energies [20]. This is why the H atom is adsorbed more stably at the TS than at the other sites.

### *Dissociation of $H_2$ molecules*

In order to study the case of the dissociation of $H_2$ molecules on the V (1 0 0) surface, the above calculation results indicate that the vertical adsorption of $H_2$ molecules is more stable than parallel adsorption; therefore we calculate the dissociation of the $H_2$ molecule from the initial adsorption at the HS on the surface, as depicted in Fig. 3. As shown, the $H_2$ molecule does not dissociate at the beginning of the HS. With gradual decreases in the vertical distance ($d_{H_2-surf}$) between the $H_2$ molecule and surface, the H—H bond begins to break. At a distance of 0.761 Å from the surface, significant H bond fracture occurs, indicating that $H_2$ dissociation depends on the initial distance of $H_2$ from the surface. The bond length, dissociation energy, and vibration frequency of a single $H_2$ molecule were calculated as 0.752 Å, 4.511 eV, and 4262 $cm^{-1}$, respectively, differing only slightly from both theoretical (respectively 0.751 Å, 4.51 eV, and 4266 $cm^{-1}$) and experimental (respectively 0.741 Å, 4.75 eV, and 4301 $cm^{-1}$) values [25,41]. Combining the adsorption energy of the H atom and $H_2$ molecule calculated above, the undissociated $H_2$ molecule is weakly physically adsorbed to the (1 0 0) surface, while the dissociated H atom is strongly chemically adsorbed. The physical adsorption energy of $H_2$ is much larger than the chemical adsorption energy of H on the (1 0 0) surface, and the relaxed and stable position is significantly different from the surface height.

### *Diffusion of H atoms*

We studied the diffusion properties of H atoms on the V surface. $H_2$ molecules at the surface of V (1 0 0) dissociate into H atoms that may diffuse either on the surface or from the surface to the subsurface, and then gradually into the interior. Using the CI-NEB method, the calculated H diffusion barrier energy is presented in Fig. 4. The number given in the figure indicates possible H diffusion paths. We first analyse Fig. 4(a), showing surface diffusion, and observe that the H diffusion barrier energy is 0.251 eV from the HS to BS, with further diffusion to the HS having a barrier energy of 0.132 eV. Thus, the total H diffusion barrier energy along the HS → BS → HS path is 0.383 eV. In addition, the H atom diffusing along the HS → TS → HS path has a diffusion barrier energy of 0.785 eV. These results indicate that the H atom preferentially diffuses along the HS → BS → HS path. Fig. 4(b) illustrates H diffusion from the surface to the first subsurface. Diffusion along the HS to TIS (1) requires an energy of 0.574 eV, while the diffusion barrier energy between the BS and TIS (1) is slightly smaller at 0.547 eV, indicating that the former path is unfavourable. We also analyse the case of diffusion from the first to second subsurface in Fig. 4 (c). The diffusion barrier energies for TIS (1) → TIS (3) through OIS (1) and TIS (1) → TIS (2) → TIS (3) are comparable at 0.464 and 0.348 eV, respectively, making the latter process energetically favourable. In conclusion, the optimal diffusion pathway for H atoms is 3 → 6 → 7 from the surface to the first subsurface to the second subsurface. This indicates that the decisive step of H atoms diffusing from the surface to subsurface is the passage through the surface of the first atomic layer. Once the H atom is below the surface, downward diffusion occurs easily. Moreover, deep diffusion of the H atom is likely to approach the diffusion energy barrier of the bulk.

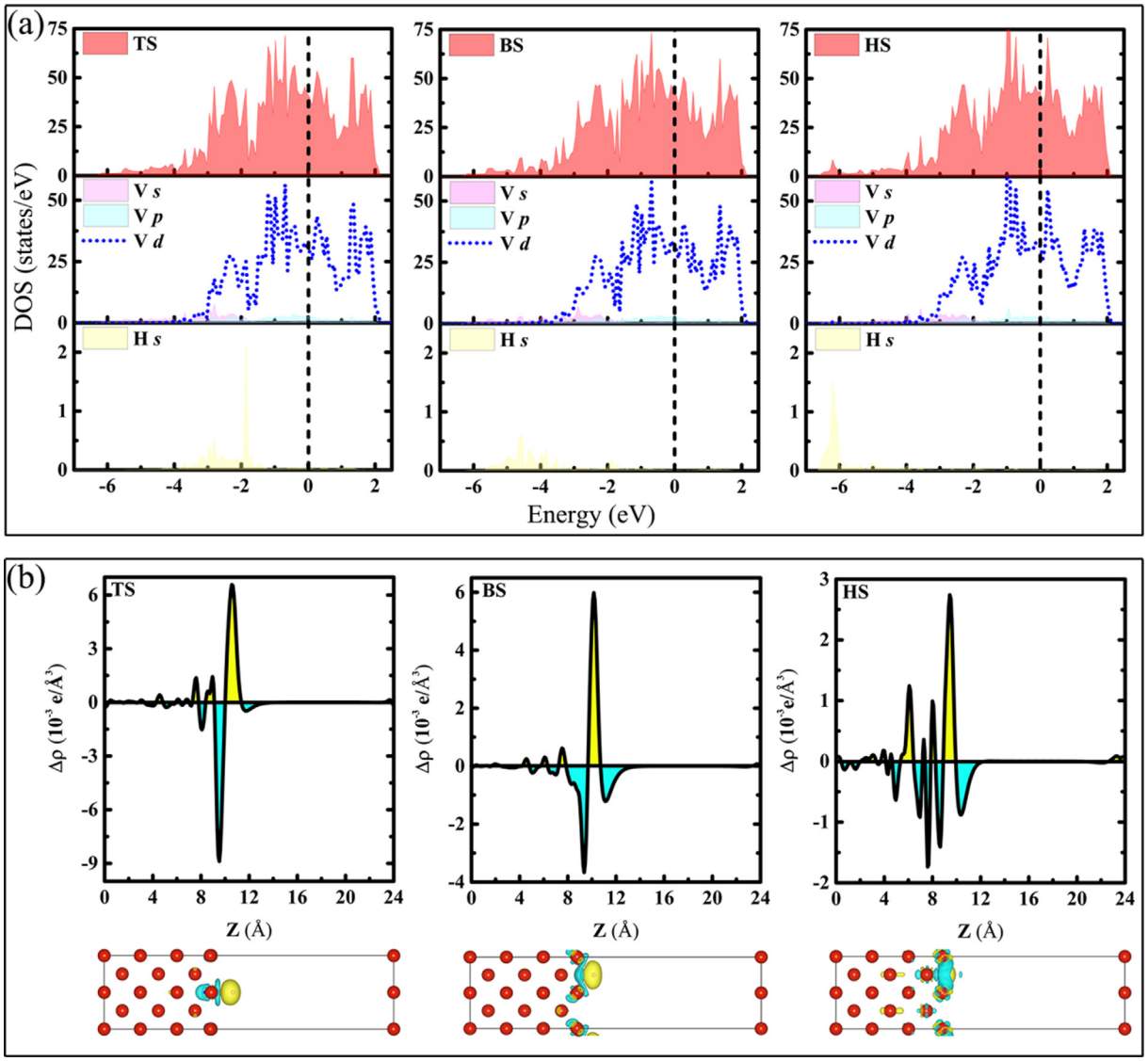


**Fig. 2.** Calculated (a) density of states and (b) plane-averaged charge density difference Δρ(z) of H atom adsorbed on the V (1 0 0) surface for TS, BS, and HS. The vertical dotted line is the Fermi level.

*Surface coverage*

We studied the effects of different surface coverage on the H adsorption energy. H coverage (θ) is defined as the ratio of the number of adsorbed H atoms (or molecules) to the number of metal atoms in each layer of the surface, considering the different permutations of H adsorption configurations. Previous calculations indicate that $H_2$ molecules are more stable when adsorbed vertically on the surface, so only the adsorption energy of vertical $H_2$ molecules on the surface is calculated here. We calculated many average adsorption energies of H atoms and molecules at different sites with changes in $0.25 < \theta \leq 1$, and found that, under the same coverage of H atoms or molecules, the adsorption energy calculated at the same adsorption sites or equivalent sites is not significantly different and that H atoms or molecules are more stable at the HS. To understand the relationship between the H atoms or molecules and coverage, the minimum adsorption energy of stable configuration is given as a function of coverage, as plotted in Fig. 5 (a, b). The adsorption energies of H atoms at the TS and BS gradually increase with increasing coverage from 0.25 to 1 ML, as indicated in Fig. 5(a). This may be attributed to electrostatic repulsion between atoms and an increased electrostatic energy, indicating the existence of repulsion between the adsorbed H atoms. The adsorption energy of H atoms adsorbed at the HS is unchanged with varying coverage, indicating that the interaction between the adsorbed H atoms is weak. Subsequently, we analyse the adsorption of $H_2$ molecules. Fig. 5(b) shows that the adsorption energy of $H_2$ decreases in the range of 0.25–0.5 ML and increases in the range of 0.5–1 ML, indicating that $\theta \leq 0.50$ ML facilitates adsorption at all three sites. For $\theta > 0.50$ ML, that is, as the number of adsorbed $H_2$ molecules increases, the stability of H molecular adsorption decreases.

*H dissolution and diffusion in bulk V*

The last issue we considered was the solubility and diffusion properties of H atoms in the bulk. When metal reacts with H to form gap-type hydrides, H generally occupies the TIS, DIS, and OIS in metal lattices. The calculated solution energy ($E_{sol}$) of H atoms in the TIS, DIS, and OIS is −0.346, −0.238, and −0.165 eV for $V_{16}H$, −0.371, −0.336, and −0.228 eV for $V_{54}H$, and −0.41, −0.336, and −0.284 eV for $V_{128}H$, respectively. Our calculations

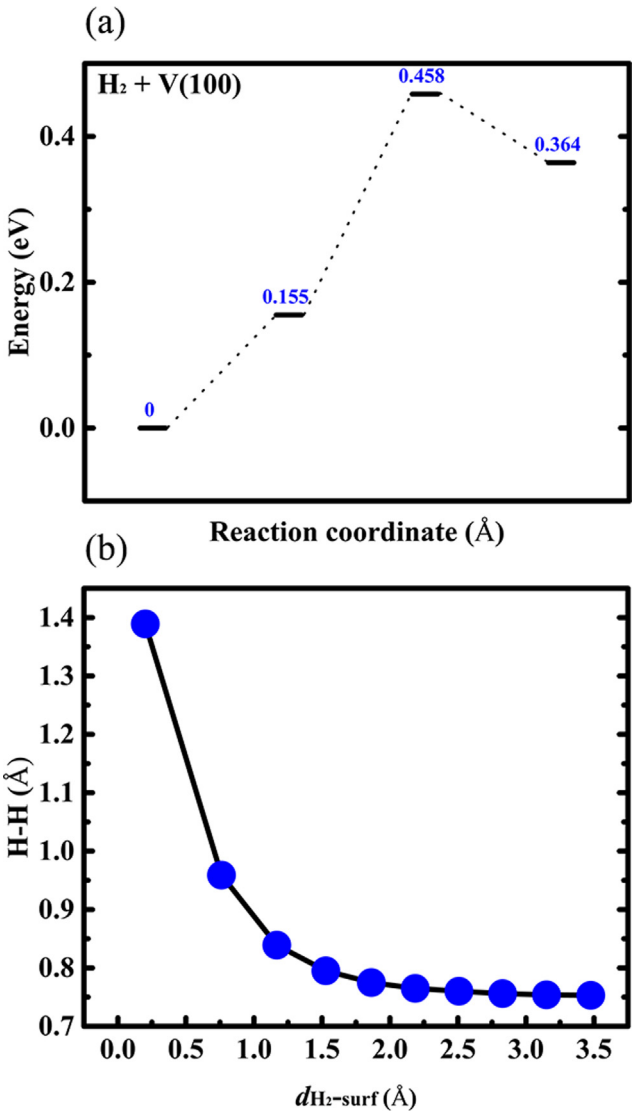


**Fig. 3.** Dissociation of $H_2$ molecules on V (1 0 0) surface: (a) reaction pathway and (b) vertical distance.

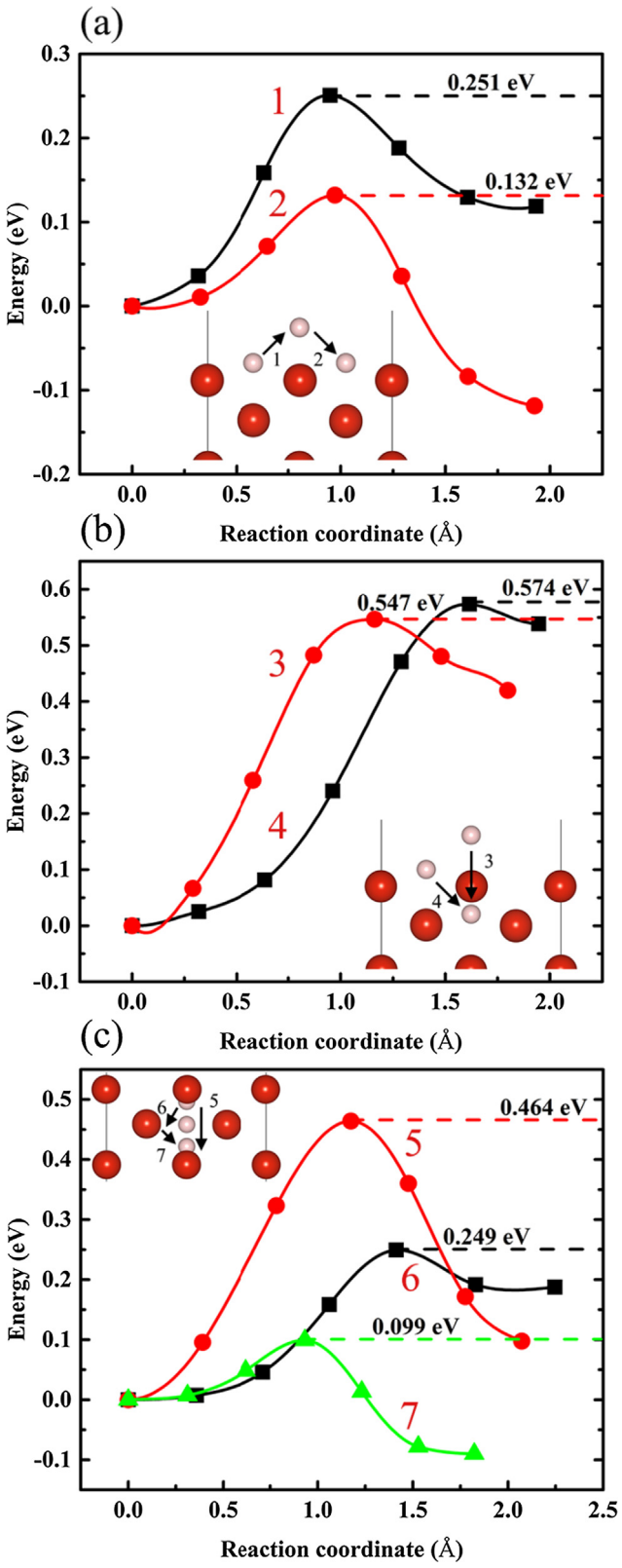


**Fig 4.** Diffusion barrier energy to H from the surface to the second subsurface. (a) Surface diffusion, (b) surface to first-subsurface diffusion, (c) and first-subsurface to second-subsurface diffusion.

are well matched to the reference values [5,14,21,22]. The $E_{sol}$ value of the TIS is much lower than those of the DIS and OIS within the entire H concentration range, implying that the most stable configuration is the TIS. Fig. 5(c) shows $E_{sol}$ of the V–H system depending slightly on the H concentration. The $E_{sol}$ values of the TIS, DIS, and OIS generally increase with H concentration, indicating that the V–H system is energetically unfavourable. We then analysed H solubility, which is critical in determining the recombination rate coefficient and is directly related to the capture and bubbling of H, as illustrated in Fig. 5(d). The concentration of H decreases as the temperature increases, indicating that the dissolution of H in V is exothermic. Moreover, H has a high concentration at room temperature, directly leading to the accumulation of H atoms at defects followed by precipitation to form $H_2$, causing the phenomenon of hydrogen embrittlement in the metal. Suzuki et al. reported that a sharp ductile-to-brittle transition occurred at ~0.2–0.25 H/M for V membranes [15].

H diffusion follows two different paths among neighbour TISs, as shown in Fig. 6. On the first path, H atoms diffuse through a DIS (see Fig. 6(a)), while on the second path, they diffuse through an OIS (Fig. 6(b)). The preferred H diffusion pathway is the first path, which is more energetically favourable than the second path. The diffusion barrier first decreases and then increases with H concentration. In addition, both the DIS and OIS are second-order

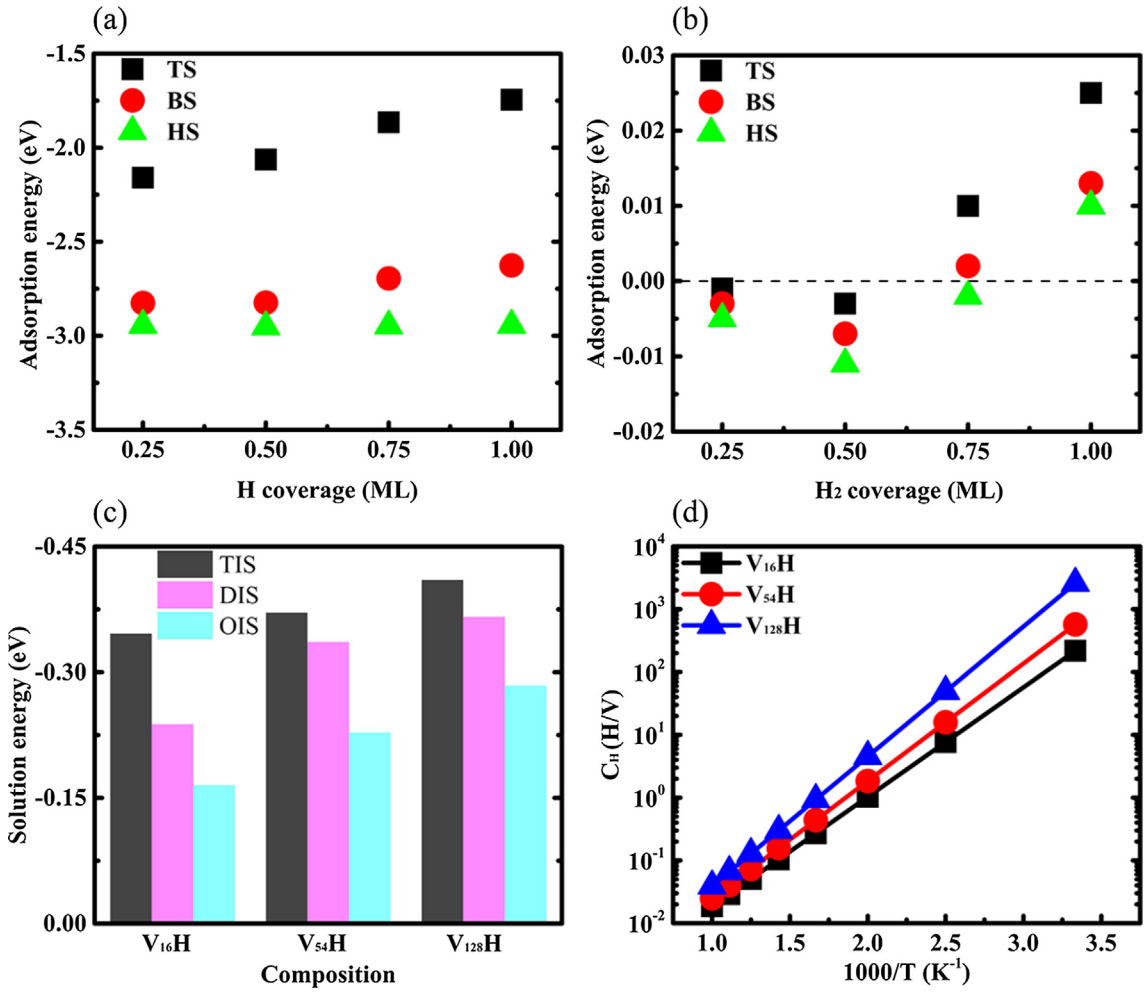


**Fig. 5.** Calculated minimum adsorption energy of the most stable configuration adsorbed on the surface of V (1 0 0) with different (a) H atom and (b) molecule coverage. Additionally, (c) solution energy and (d) solubility coefficient of H in the bulk.

saddle points on the potential energy surface. Sorescu et al. also proved such a case occurring in bcc bulk Fe [26]. Consequently, H diffusion mainly occurs between adjacent TISs. We further discussed the diffusion coefficient of H, which measures the ability of H atoms to diffuse across a metallic membrane. To match the experimental components and enable comparison [4,7], we chose to study the diffusion coefficient of H in the $V_{16}H$ phase using the Arrhenius diffusion equation [42,43], as illustrated in Fig. 6 (c). At an operating temperature of 673 K, the value is $1.73 \times 10^{-8}$ - $m^2\ s^{-1}$, unlike the existing experimental and calculated values of $1.2 \times 10^{-8}$ [7] and $1.25 \times 10^{-8}\ m^2\ s^{-1}$ [4], respectively. This may arise from differences in calculations and experiments, especially in the activation barrier of H. In addition, the diffusivity increases with temperature.

## Conclusion

In summary, we have employed a combination of first-principles methods and empirical theory to study the adsorption, dissociation, and diffusion properties of H on the V (1 0 0) surface and in the bulk. Our calculation results indicate that the most stable adsorption configuration with different coverages of H atoms and molecules on the surface is the HS. Specifically, the HS is the most thermodynamically stable site for H atom adsorption, with an almost constant adsorption energy at 0.25–1 ML coverage. $H_2$ molecules tend to become adsorbed vertically at the HS on the surface, showing a very weak physical adsorption state. With increasing coverage, the adsorption energy first decreases and then decreases. In addition, $H_2$ molecules gradually dissociate into H atoms as they approach the surface. The diffusion of H atoms on the surface, from the surface to the first subsurface, and from the first subsurface to the second subsurface, optimally occurs via the paths of HS → BS → HS, BS → BS, and BS → TIS → BS, respectively. For the bulk, we find that H atoms occupy the most stable TIS and diffuse along adjacent TISs. At the operating temperature of 673 K, the H diffusion coefficient is $1.73 \times 10^{-8}\ m^2\ s^{-1}$ for $V_{16}H$. This study is important for the next step of alloying element doping, regulation, and Pd plating to obtain better H permeability in membrane metals.

## Compliance with ethics requirements

This article does not contain any studies with human or animal subjects.

## Declaration of Competing Interest

The authors declare that they have no conflicts of interest.

## Acknowledgments

This work was financially supported by the National Natural Science Foundation of China (Nos. 51471055, 11464008, 51401060, 51761007, 51961010, 51801163, and 51901054), the

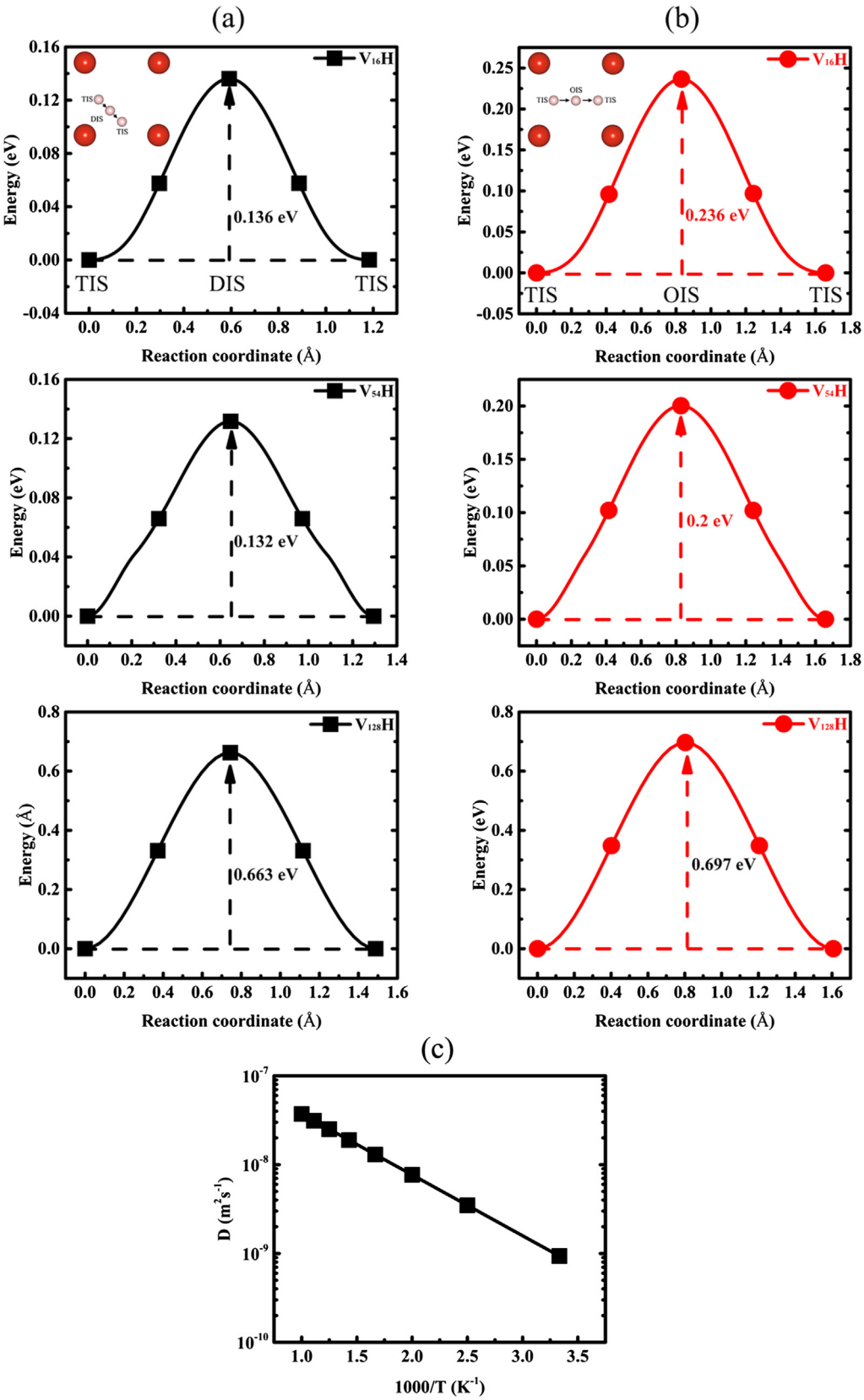


**Fig. 6.** Calculated (a) TIS → DIS → TIS and (b) TIS → OIS → TIS of diffusion barrier energy of H in pure V as a function of H concentration, as well as (c) diffusion coefficient of H in pure V as a function of reciprocal temperature.

Natural Foundations of Guangxi Province (Nos. 2014GXNSFGA118001 and 2016GXNSFGA380001), Guangxi Key Laboratory of Information Materials (171001-Z), Guangxi Postgraduate Innovation Project (YCSW2018144), and Guangxi Science and Technology Project (GuiKeAB182810103).

## References

[1] Xu ZJ, Wang ZM, Tang JL, Deng JQ, Yao QR, Zhou HY. Effects of Mo alloying on the structure and hydrogen-permeation properties of Nb metal. J Alloy Compd 2018;740:810–5.
[2] Semidey-Flecha Lymarie, Sholl DS. Combining density functional theory and cluster expansion methods to predict $H_2$ permeance through Pd-based binary alloy membranes. J Chem Phys 2008;128:144701.
[3] Hao Chongyan, Wu Yang, An Yajing, Cui Baihua, Lin Jiannan, Li Xiaoning, Wang Dianhui, Jiang Minhong, Cheng Zhenxiang, Hu Shi. Interface-coupling of CoFe-LDH on MXene as high-performance oxygen evolution catalyst. Mater Today Energy 2019;12:453–62. https://linkinghub.elsevier.com/retrieve/pii/S246860691930036X. doi: https://doi.org/10.1016/j.mtener.2019.04.009.
[4] Dolan MD. Non-Pd BCC alloy membranes for industrial hydrogen separation. J Membr Sci 2010;362:12–28.
[5] Alimov VN, Bobylev IV, Busnyuk AO, Notkin ME, Peredistov EY, Livshits AI. Hydrogen transport through the tubular membranes of V-Pd alloys: permeation, diffusion, surface processes and WGS mixture test of membrane assembly. J Membr Sci 2018;549:428–37.
[6] Rochana P, Lee K, Wilcox J. Nitrogen adsorption, dissociation, and subsurface diffusion on the vanadium (110) surface: a DFT study for the nitrogen-selective catalytic membrane application. J Phys Chem C 2014;118:4238–49.
[7] Liu F, Xu ZJ, Wang ZM, Dong MY, Deng JQ, Yao QR, et al. Structures and mechanical properties of Nb-Mo-Co (Ru) solid solutions for hydrogen permeation. J Alloy Compd 2018;756:26–32.
[8] Kumar S, Jain A, Ichikawa T, Kojima Y, Dey GK. Development of vanadium-based hydrogen storage material: a review. Renew Sust Energy Rev 2017;72:791–800.
[9] Qin JY, Wang ZM, Wang DH, Wu Y, Zhong Y, Hu CH, et al. Dissolution, diffusion, and penetration of H in the group VB metals investigated by first-principles method. Int J Hydrogen Energy 2019. doi: https://doi.org/10.1016/j.ijhydene.2019.03.228.
[10] Gui LJ, Liu YL, Wang WT, Jin S, Zhang Y, Lu GH, et al. First-principles investigation on vacancy trapping behaviors of hydrogen in vanadium. J Nucl Mater 2013;442:S688–93.
[11] Dolan MD, Viano DM, Langley MJ, Lamb KE. Tubular vanadium membranes for hydrogen purification. J Membr Sci 2018;549:306–11.
[12] Sakaki K, Kim H, Iwase K, Majzoub EH, Machida A, Watanuki T, et al. Interstitial-atom-induced phase transformation upon hydrogenation in vanadium. J Alloy Compd 2018;750:33–41.
[13] Luo J, Zhou HB, Liu YL, Gui LJ, Jin S, Zhang Y, et al. Dissolution, diffusion and permeation behavior of hydrogen in vanadium: a first-principles investigation. J Phys-Condens Mat 2011;23:135501.
[14] Zhang P, Zhao J, Wen B. Trapping of multiple hydrogen atoms in a vanadium monovacancy: a first-principles study. J Nucl Mater 2012;429:216–20.
[15] Suzuki A, Yukawa H, Ijiri S, Nambu T, Matsumoto Y, Murata Y. Alloying effects on hydrogen solubility and hydrogen permeability for V-based alloy membranes. Mater Trans 2015;56:1688–92.
[16] Ko WS, Shim JH, Jung WS, Lee BJ. Computational screening of alloying elements for the development of sustainable V-based hydrogen separation membranes. J Membr Sci 2016;497:270–81.
[17] Koller R, Bergermayer W, Kresse G, Hebenstreit ELD, Konvicka C, Schmid M, et al. The Structure of the Oxygen Induced (1×5) Reconstruction of V(100). Surf Sci 2001;480:11–24.
[18] Davies PW, Lambert RM. Another unique reconstruction of the V(100) surface: p(2×2) microfacets on a (111) oriented crystal. Chem Phys Lett 1981;83:480–2.
[19] Wu Y, Wang ZM, Liu PF, Bo T, Hao CY, Hu CH, et al. Understanding of transition metal (Ru, W) doping into Nb for improved thermodynamic stability and hydrogen permeability: density functional theory calculations. Phys Chem Chem Phys 2019. doi: https://doi.org/10.1039/c9cc02012h.
[20] Hua J, Liu YL, Li HS, Zhao MW, Liu XD. Effect of the alloying element titanium on the stability and trapping of hydrogen in pure vanadium: a first-principles study. Int J Mod Phys B 2014;28:1450207.
[21] Ouyang C, Lee YS. Hydrogen-induced interactions in vanadium from first-principles calculations. Phys Rev B 2011;83:45111.
[22] Qin JY, Wang ZM, Wang DH, Wang F, Yan X, Zhong Y, et al. First-principle investigation of hydrogen solubility and diffusivity in transition metal-doped vanadium membranes and their mechanical properties. J Alloy Compd 2019;805:747–56.
[23] Vitos L, Ruban AV, Skriver HL, Kollar J. The surface energy of metals. Surf Sci 1998;411:186–202.
[24] Nojima A, Yamashita K. A theoretical study of hydrogen adsorption and diffusion on a W (1 1 0) surface. Surf Sci 2007;601:3003–11.
[25] Gong L, Su Q, Deng H, Xiao S, Hu W. The stability and diffusion properties of foreign impurity atoms on the surface and in the bulk of vanadium: a first-principles study. Comp Mater Sci 2014;81:191–8.
[26] Sorescu DC. First principles calculations of the adsorption and diffusion of hydrogen on Fe (1 0 0) surface and in the bulk. Catal Today 2005;105:44–65.
[27] Wu Y, Wang ZM, Wang DH, Qin JY, Wan ZZ, Zhong Y, et al. First-principles investigation of atomic hydrogen adsorption and diffusion on/into Mo-doped Nb (100) surface. Appl Sci 2018;8:2466.
[28] Kresse G, Hafner J. Ab-initio molecular dynamics for liquid metals. Phys Rev B 1993;47:558–61.
[29] Kresse G, Furthmüller J. Efficient iterative schemes for ab initio total-energy calculations using a plane-wave basis set. Phys Rev B 1996;54:11169–86.
[30] Perdew JP, Wang Y. Accurate and simple analytic representation of the electron-gas correlation energy. Phys Rev B 1992;45:13244–9.
[31] Blöchl PE. Projector augmented-wave method. Phys Rev B 1994;50:17953–79.
[32] Perdew JP, Burke K, Ernzerhof M. Generalized gradient approximation made simple. Phys Rev Lett 1998;77:3865–8.
[33] Henkelman G, Uberuaga BP, Jonsson H. A climbing image nudged elastic band method for finding saddle points and minimum energy paths. J Chem Phys 2000;113:9901–4.
[34] Li Q, Rellán-Piñeiro M, Almora-Barrios N, Garcia-Ratés M, Remediakis IN, López N. Shape control in concave metal nanoparticles by etching. Nanoscale 2017;9:13089–94.
[35] Li X, Zhang H, Lu S, Li W, Zhao J, Johansson B, et al. Elastic properties of vanadium-based alloys from first-principles theory. Phys Rev B 2012;86:014105.
[36] Bolef DI, Smith RE, Miller JG. Elastic properties of vanadium. I. Temperature dependence of the elastic constants and the thermal expansion. Phys Rev B 1971;3:4100.
[37] Lee JY, Punkkinen MPJ, Schönecker S, Nabi Z, Kádas K, Zólyomi V, et al. The surface energy and stress of metals. Surf Sci 2018;674:51–68.
[38] Ferrin P, Kandoi S, Nilekar AU, Mavrikakis M. Hydrogen adsorption, absorption and diffusion on and in transition metal surfaces: a DFT study. Surf Sci 2012;606:679–89.
[39] Xia C, Du J, Xiong W, Jia Y, Wei Z, Li J. A type-II GeSe/SnS heterobilayer with a suitable direct gap, superior optical absorption and broad spectrum for photovoltaic applications. J Mater Chem A 2017;5:13400–10.
[40] Liu J. Origin of high photocatalytic efficiency in monolayer g-$C_3N_4$/CdS heterostructure: a hybrid DFT study. J Phys Chem C 2015;119:28417–23.
[41] Huber KP, Herzberg G. Molecular Spectra and Molecular Structure 4: Constants of Diatomic Molecules. New York: Van Norstrand Reinhold Co; 1979.
[42] Wu Y, Wang ZM, Wang DH, Wan ZZ, Zhong Y, Hu CC, et al. Effects of Ni doping on various properties of NbH phases: a first-principles investigation. Sci Rep 2017;7:6535.
[43] Wang DH, Wu Y, Wan ZZ, Wang F, Wang ZM, Hu CH, et al. Effects of Mo alloying on stability and diffusion of hydrogen in the $Nb_{16}H$ phase: a first-principles investigation. RSC Adv 2019;9:19495–500.